Kannan, Jeevananthan; Gadalla, Mahmoud; Tekgül, Bulut; Karimkashi, Shervin; Kaario, Ossi; Vuorinen, Ville

Large eddy simulation of diesel spray–assisted dual-fuel ignition

Published in:
International Journal of Engine Research

DOI:
10.1177/1468087420946551

Published: 10/08/2020

Document Version
Peer-reviewed accepted author manuscript, also known as Final accepted manuscript or Post-print

Please cite the original version:
Kannan, J., Gadalla, M., Tekgül, B., Karimkashi, S., Kaario, O., & Vuorinen, V. (2020). Large eddy simulation of diesel spray–assisted dual-fuel ignition: A comparative study on two n-dodecane mechanisms at different ambient temperatures. *International Journal of Engine Research*, Article 1468087420946551.
https://doi.org/10.1177/1468087420946551

Journal Title
XX(X):1–11

DOI: 10.1177/ToBeAssigned
www.sagepub.com/
SAGE

Large-eddy simulation of diesel spray assisted dual-fuel ignition: A comparative study on two n-dodecane mechanisms at different ambient temperatures

Jeevananthan Kannan[1], Mahmoud Gadalla[1], Bulut Tekgül[1], Shervin Karimkashi[1], Ossi Kaario[1], Ville Vuorinen[1]

Abstract

In dual-fuel (DF) compression ignition (CI) engines, a high-reactivity fuel (HRF), such as diesel, is directly injected to the engine cylinder to ignite a mixture of low-reactivity fuel (LRF) and air. This study targets improving the general understanding on the DF ignition phenomenon using zero-dimensional (0D) homogeneous reactor studies and three-dimensional (3D) large eddy simulation (LES) together with finite-rate chemistry. Using the LES framework, n-dodecane liquid spray is injected into the lean ambient methane-air mixture at $\phi = 0.5$. The injection conditions have a close relevance to the ECN Spray A setup. Here, we assess the effect of two different chemical mechanisms on ignition characteristics: a skeletal mechanism with 54 species and 269 reaction steps (Yao mechanism) and a reduced mechanism with 96 species and 993 reaction steps (Polimi mechanism). Altogether three ambient temperatures are considered: 900, 950, and 1000 K. Longer ignition delay time (IDT) is observed in 3D LES spray cases compared to 0D homogeneous reactors, due to the time needed for fuel mixing in 3D LES sprays. Although ignition is advanced with the higher ambient temperature using both chemical mechanisms, the ignition process is faster with the Polimi mechanism compared to the Yao mechanism. The reasons for differences in ignition timing with the two mechanisms are discussed using the 0D and 3D LES data. Finally, heat release modes are compared in 3D LES according to low- and high-temperature chemistry in DF combustion at different ambient temperatures. It is found that Yao mechanism overpredicts the first-stage ignition compared to Polimi mechanism, which leads to the delayed second-stage ignition in Yao cases compared to Polimi cases. However, the differences in DF ignition for Polimi and Yao mechanisms are relatively smaller at higher ambient temperatures.

Keywords
Dual-fuel, LES, ECN, Spray A, Combustion, Ignition

Introduction

Several clean combustion technologies have been recently developed in order to reduce particulates, NOx, and greenhouse gas emissions. In this respect, there have been considerable improvements in engine technologies such as the utilization of renewable fuels, electrification, and development of hybrid engines. Recently, in the context of compression ignition (CI) engines, more advanced combustion strategies such as dual-fuel (DF) combustion have been proposed and used as viable solutions to provide higher efficiency and lower emissions compared to the conventional CI engines[1–5]. The idea of DF combustion in CI engines is to burn one (or a combination of) low reactivity fuel(s) (LRF), such as methane, with the assistance of a high reactivity fuel (HRF), such as diesel. With relevance to this study, pilot HRF is injected to the lean mixture of premixed LRF/air to initiate ignition and burn interactively with LRF[1–3,6–11]. Typically, diesel is injected in small amounts to avoid high emissions, however, it should release sufficient energy to ignite the LRF under desired conditions.

The present study is linked to the previous research by Kahila et al.[2] and Tekgul et al.[3] where DF spray ignition was numerically explored in the Engine Combustion Network (ECN) Spray A context[2,12–17]. In this configuration, a low- temperature (363 K) liquid n-dodecane is sprayed to the high-temperature ambient of premixed methane/air at ϕ=0.5. The present study seeks to investigate the effect of chemical kinetics mechanism on DF spray ignition in three-dimensional (3D) large-eddy simulations LES/finite-rate chemistry modeling context at various temperatures. Here, methane is considered as the LRF and n-dodecane is the diesel surrogate considered as the HRF. We note that n-dodecane has similar thermochemical properties to

---

[1] Aalto University, Department of Mechanical Engineering, School of Engineering, Otakaari 4, 02150, Espoo, Finland

Corresponding author:
Jeevananthan Kannan, Energy Conversion Group, Aalto University, Department of Mechanical Engineering, School of Engineering, Otakaari 4, 02150, Espoo, Finland
Email: jeevananthan.kannan@aalto.fi

diesel and methane has a low carbon content which leads to lower carbon dioxide emissions (CO_2) compared to long hydrocarbons such as diesel. Additionally, the abundant availability of methane in nature, its relatively low price, and the wide infrastructure of methane gas distribution network around the globe are the main motivations in using methane as LRF in DF CI engines[8,18,19].

Several experimental[20–23] studies have investigated ambient temperature effects on single fuel (SF) n-dodecane ignition in the ECN Spray A configuration. Such studies have reported longer ignition delay time (IDT) at lower ambient temperatures due to the longer mixing timescales and chemistry slow-down. Even though there has been growing interest in DF combustion research, the literature indicates that the main focus has been on the performance and emission characteristics of CI engines. Only recently, investigation of ignition characteristics in DF engines has been considered in the literature. In rapid compression-expansion machine (RCEM) experiments[24,25], it was noted that diesel ignition is retarded in DF (premixed methane-air) compared to SF mode (pure air ambient). For instance, Srna et al.[25] performed laser diagnostics on RCEM experiments to identify the early low-temperature ignition stage using formaldehyde detection. They found that both low- and high-temperature ignition are delayed with the presence of methane in combustion. Also, their findings indicate that methane has a more significant retarding effect on DF ignition at lower ambient temperatures.

Moreover, several numerical studies have similarly reported IDT delay in the DF mode compared to the SF mode, which span from zero-dimensional (0D) to spray-assisted 3Dd DF ignition studies[26–33]. There are also a few studies that scrutinized turbulence modelling through Reynolds average Navier-Stokes (RANS) approach[26,27,34]. In such a RANS modelling approach, combustion phenomenon was studied using finite rate chemistry and experimental in-cylinder pressure data was used for the validation purpose. In addition, few studies have reported DF ignition characteristics using direct numerical simulations (DNS), e.g.[30,32,33]. For instance, Demosthenous et al.[32] have studied ignition of n-heptane droplets in premixed methane/air ambient with the presence of decaying homogeneous isotropic turbulence. More recently, Kahila et al.[2,35] and Tekgul et al.[3] numerically investigated dual-fuel ignition of a diesel spray in methane-air mixture. With relevance to this study, Tekgul et al.[3] have shown that the retarding effect of methane is stronger at lower ambient temperatures and their chemical sensitivity analysis indicated that methane oxidation reactions are more important at lower temperatures.

Despite the mentioned literature on DF combustion investigation under various initial conditions, the literature review indicates the following research gaps. First, the influence of utilized chemical kinetics mechanisms on numerical simulations of DF ignition is not thoroughly reported. Determination of the DF ignition sensitivity to the utilized chemical kinetics mechanisms in the literature is in particular important because most of these chemical mechanisms are developed for SF ignition. Second, a detailed analysis of DF ignition characteristics with different ambient temperature using different chemical mechanisms is not presented in the literature. In this study, LES of DF ignition are carried out in the context of modified ECN Spray A baseline conditions using two different chemical kinetics mechanisms and at three different initial ambient temperatures; in total six LES case studies. Additionally, DF ignition characteristics are investigated using 0D homogeneous reactor computations to compare with LES findings. Therefore, main objectives of the present work are to: (i) understand DF ignition characteristics at engine relevant conditions using homogeneous reactor computations and 3D LES, (ii) investigate DF ignition deviations between two chemical mechanisms for ambient temperatures ranging between 900 and 1000 K, and (iii) identify combustion modes and high-temperature chemistry (HTC) and low-temperature chemistry (LTC) at different ambient temperatures.

Numerical Methodology

In the present study, Navier-Stokes equations for gas phase compressible turbulent flow are solved using the LES approach. The present numerical strategy has been thoroughly validated in our previous publications for the SF ECN Spray A case[17,36–38] and SF/DF cases[2,3]. The solver provides results in a very good agreement with the ECN data in terms of the liquid length, vapor penetration, radial mixture fraction profiles, and ignition characteristics. According to Kahila et al.[2,35], the Favre-filtered LES formulation for continuity, momentum and energy equations are given below.

$$\frac{\partial \bar{\rho}}{\partial t} + \frac{\partial \bar{\rho} \tilde{u}_i}{\partial x_i} = \bar{S}_\rho, \tag{1}$$

$$\begin{aligned} &\frac{\partial (\bar{\rho} \tilde{u}_i)}{\partial t} + \frac{\partial (\bar{\rho} \tilde{u}_i \tilde{u}_j)}{\partial x_j} = \\ &\frac{\partial}{\partial x_j} (-\bar{p}\delta_{ij} + \bar{\rho} \tilde{u}_i \tilde{u}_j - \bar{\rho} \widetilde{u_i u_j} + \bar{\tau}_{ij}) + \overline{S}_{u_i}, \end{aligned} \tag{2}$$

$$\begin{aligned} &\frac{\partial (\bar{\rho} \widetilde{Y_k})}{\partial t} + \frac{\partial (\bar{\rho} \tilde{u}_i \widetilde{Y_k})}{\partial x_i} = \\ &\frac{\partial}{\partial x_i} \left(\bar{\rho} \tilde{u}_i \widetilde{Y_k} - \bar{\rho} \widetilde{u_i Y_k} + \bar{\rho} \widetilde{D} \frac{\partial \widetilde{Y_k}}{\partial x_i} \right) + \overline{S}_{Y_k} + \bar{\dot{\omega}}_k, \end{aligned} \tag{3}$$

$$\begin{aligned} &\frac{\partial (\bar{\rho} \widetilde{h_t})}{\partial t} + \frac{\partial (\bar{\rho} \widetilde{u_j} \widetilde{h_t})}{\partial x_j} = \\ &\frac{\partial \bar{p}}{\partial t} + \frac{\partial}{\partial x_j} \left(\bar{\rho} \widetilde{u_j} \widetilde{h_s} - \bar{\rho} \widetilde{u_j h_s} + \frac{\overline{\lambda}}{\overline{c_p}} \frac{\partial \widetilde{h_s}}{\partial x_j} \right) + \overline{S}_h + \bar{\dot{\omega}}_h, \end{aligned} \tag{4}$$

where $\overline{\rho}, \widetilde{u_i}, \overline{p}, \overline{Y_k}, \widetilde{h_s}\ and\ \overline{\tau_{ij}}$, denote the filtered density, velocity, pressure, k^{th} species mass fraction, sensible enthalpy and viscous stress tensor, respectively. Here, $\sim$

represents density-weighted ensemble average while the over-bar denotes unweighted average. Moreover, Lewis number of unity is assumed for all species. Source terms of $\overline{S_\rho}, \overline{S_{u,i}}, \overline{S_{Y_k}}$ and $\overline{S_{Y_k}}$ provide coupling between the liquid and gaseous phases with respect to mass, momentum, species and energy, respectively. The production rate of the species k and heat release rate (HRR) are denoted by $\overline{\dot{\omega_k}}$ and $\overline{\dot{\omega_h}}$, respectively. The above-mentioned governing equations are closed by the filtered ideal gas law. The governing equations are solved using the finite volume library OpenFOAM[39]. Here, a second order time integration method is utilized whereas the pressure-velocity coupling is treated using the PIMPLE algorithm[2,3,17,38].

In the present 3D simulations, implicit LES (ILES) is used as a "stand-alone" turbulence model without any explicit subgrid scale turbulent dissipation. In practice, the ILES is implemented by discretizing the convection terms by a flux limited interpolation while the diffusive fluxes are linearly interpolated. Here, consistent with our previous works[2,3,17,40], the Gamma scheme, a non-linear flux limited scheme of 2nd order spatial accuracy is used to discretize the convective fluxes[41]. The Gamma scheme requires an input parameter k which is chosen to control the level of numerical diffusion. Here, we choose $k = 0.3$ for the momentum equation whereas $k = 1.0$ is selected for the scalars ensuring a bounded total variation diminishing solution. These k values are selected based our previous studies[2,3,17,38]. We note that recently Gadalla et al.[38] compared the ILES approach against different SGS models in the ECN Spray A context, while Kaario et al. 2020[42] studied effects of multiple flow realizations on LES results. It was shown that the ILES approach and flow realizations have minimal effects on the results of the spray A LES.

For the injected liquid phase modeling, the Lagrangian particle tracking (LPT) method is applied with a similar model setup as in our previous Spray A studies[2,35,38]. Instead of modeling the secondary breakup, we use a constant initial droplet diameter $(0.5\mu\mathrm{m})$ as justified and explained in our previous papers[38,42]. The standard correlations of Ranz and Marshall[43] and Frossling[44] are used for modeling heat and mass transfer between the liquid and gas phases. Similar to our previous studies[2,3,35], no model for turbulence chemistry interactions (TCI) is considered. Additionally, the ambient mixture composition and temperature are initiated as uniform fields while the velocity field is set to zero. The injection profile is adopted from a virtual profile generator, as suggested by the ECN.

For finite-rate chemistry/LES simulations, we have coupled the open-source library pyJac[45] with OpenFOAM. The pyJac package provides the reaction rate coefficients along with the analytical Jacobian matrix formulation required by the ordinary differential equation (ODE) system solver. Moreover, dynamic load balancing is employed to accelerate the computational process as further explained by Kahila et al.[35]. Species transport equations, which include details of multiple species transport and reaction pathways, are considered in this study. These species transport equations are solved using finite-rate chemistry model, which is the preferred method in terms of accuracy and availability in modern numerical computations[35]. More details and validation on the pyJac-OpenFOAM coupling have been provided in our previous works[2,35].

Table 1. Specifications of DF Spray simulations as compared to the ECN Spray A conditions.

	ECN Spray A	**DF**
Injection parameters		
Fuel	n$-C_{12}H_{26}$	n$-C_{12}H_{26}$
Nozzle diameter	$90\mu m$	$90\mu m$
Temperature	363 K	363 K
Pressure	150MPa	150MPa
Ambient conditions		
Temperature	900 K	900, 950, 1000 K
Density	22.8 kg/m^3	22.8 kg/m^3
O_2(molar)	15.0 %	15.0 %
CO_2(molar)	6.230 %	5.955 %
H_2O(molar)	3.620 %	3.460 %
N_2(molar)	75.150 %	71.835 %
CH_4(molar)	-	3.750 %
ϕ	0	0.5

Here, two different chemical kinetics mechanisms are considered; Yao mechanism (54 species and 269 reaction steps)[46] and Polimi reduced mechanism (96 species and 993 reaction step)[47], hereafter called Yao and Polimi respectively. Although both chemical mechanisms are originally developed for single-fuel n-dodecane combustion under the ECN Spray A conditions, they are previously used in the DF ignition context[2,3,35,48,49]. Due to the lack of DF experimental data under engine-relevant conditions, validations are only performed against available data for single-fuel methane and n-dodecane combustion in our earlier works,[2,3]. Here, the main goal is to understand the differences in ignition characteristics of Yao compared with Polimi in a range of relevant ambient temperatures. Computational costs of the carried out 3D LES studies with Yao and Polimi are compared and reported in Appendix B. As shown in Appendix B, the computational load per timestep depends on the chosen chemical mechanism as well as the temperature level. We note that Yao mechanism is by almost factor 2 faster than Polimi mechanism at each respective ambient temperature.

Simulation configuration

The present 3D simulation configuration is based on the ECN Spray A experimental setup modified for DF studies. The setup was first introduced by Kahila et al.[2]. In the present modified DF setup, similar to the SF ECN Spray A setup, n-dodecane is injected from a 90-micron diameter nozzle at pressure of 150 MPa into a chamber at ambient temperature T_a= 900 K. In the present study, the molar composition of O_2 in the chamber is set initially to 15%. Here, according to Kahila et al.[2], the above-mentioned conditions are modified for DF studies and the equivalence ratio of the premixed methane-air mixture is set to 0.5. Here, T_a =900, 950 and 1000 K while the chamber pressure is initially p_a = 60bar. The molar concentration of O_2 is initialized at 15%, and the other molar compositions are modified accordingly as reported in Table 1 compared to the baseline ECN Spray A. The volume of the computational domain used in the present LES matches the experimental combustion chamber volume of the Sandia National Laboratory[3,35].

Here, three different refinement regimes are considered to capture the main physics and chemistry of the ignition process. There are altogether three grid refinement zones in present simulations as displayed along with the computational domain in Figure 1. Here, region R1 has a grid spacing of 1mm and this region is far from the diesel spray. Also, regions R2 and R3 have uniform grid spacing of 250 and 125 microns, and they are extended 65 mm and 32 mm downstream of the nozzle, respectively. We note that R3 region has the finest grid resolution, such that it can capture the intense mixing of n-dodecane spray with the premixed methane-air ambient. The present mesh resolution has been used and validated in our previous non-reactive cases[37,42]. A separate mesh sensitivity analysis is provided in Appendix A, which is focusing on the region R3.

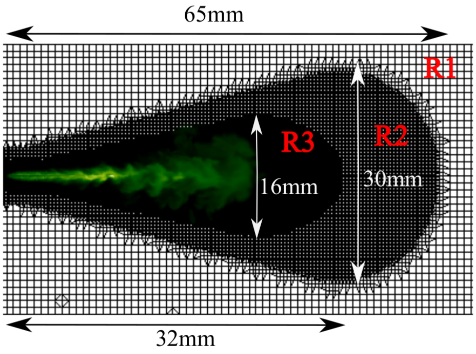

Figure 1. The computational domain used in the present work. Mixture fraction field is shown in the background. R3, R2 and R1 regions correspond to uniform resolution of 125 micron, 250 micron, and 1 mm grid spacing, respectively.

Results and Discussion

Overview on 3D spray ignition

Based on our 3D LES data, characteristic features of DF ignition using Polimi and Yao at 900 K ambient temperature are schematically illustrated in Figure 2. Mixing and ignition phenomena can be observed through three different distinguished zones as marked in this figure. In the mixing and evaporation zone (I), liquid droplets accelerate the gas stream which becomes turbulent and leads to entrainment of the hot ambient gases to the spray axis enhancing rapid evaporation and termination of the liquid phase at the liquid length. Then, the evaporated gaseous n-dodecane stream mixes intensely with the methane-air mixture forming the low-temperature chemistry (LTC) zone (II). LTC reactions lead to the decomposition of the long hydrocarbon n-dodecane and consequently, intermediate radical species such as $C_{12}H_{25}O_2$, called RO_2 hereafter, are formed[50] leading to the first-stage ignition. Finally, downstream of the LTC zone, high-temperature chemistry (HTC) zone (III) involves HTC reactions which complete the oxidation process leading to the second-stage ignition. The HTC zone involves reactions with OH production/consumption. In this zone, temperature levels increase significantly leading to the ignition in the vicinity of the spray (HTC region).

In this study, the first-stage IDT (τ_1) is defined as the characteristic time for onset of low-temperature chemistry (LTC) reactions, and it is defined as the time instance at which 20 % maximum value of RO_2 is reached[35]. The second-stage IDT (τ_2) is defined as the time instance when maximum of temperature gradient is observed which represents initiation of HTC reactions.

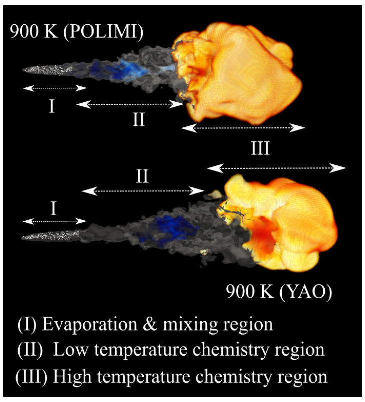

Figure 2. N-dodecane spray ignition process in ambient methane/air (DF) at 900 K ambient temperature using Polimi and Yao. Visualizations are taken at 1.1 IDT.

0D homogenous reactor analysis

Prior to the presentation of 3D LES simulations, we study ignition characteristics of DF combustion by 0D homogeneous reactor calculations considering the adiabatic mixing line concept[51]. In the mixing line concept, the main idea is to consider enthalpy-based inert mixing of two presumed streams before the simulation. Here, the gas stream of methane/air ($\phi = 0.5$, T_a =900, 950, and 1000 K) and n-dodecane fuel stream ($T_a = 363$ K) are mixed at different mixture fraction values in 0D homogeneous reactor at 60 bar. Here, 0D homogeneous reactor simulations are carried out using Cantera with two different n-dodecane chemical mechanisms: Polimi and Yao. Mixture fraction, ξ, which describes the mixing extent of liquid fuel stream and the premixed oxidizer stream is defined by Equation 5 based on mass fraction of N_2, and it is consistent with the definition provided by Bilger et al.[52].

$$\xi = \frac{Y_{N_2} - Y_{N_2^{ox}}}{Y_{N_2^{f}} - Y_{N_2^{ox}}} \tag{5}$$

Additionally, the most reactive mixture fraction (ξ_{MR}) is defined as the shortest IDT within the tested range of ξ. Table 2 presents ξ_{MR} values from 0D homogeneous reactor calculations at different T_a using both Yao and Polimi mechanisms. In addition, DF ignition characteristic values at ξ_{MR} using the two selected chemical mechanisms are summarized in Table 3.

Figure 3 displays IDT of DF mixtures along the mixing line as a function of mixture fraction ξ for different ambient temperatures with Polimi and Yao. The following

Table 2. ξ_{MR} values from 0D homogeneous reactor calculations using Polimi and Yao chemical mechanisms.

	900 K	950 K	1000 K
ξ_{MR} (Polimi)	0.088	0.105	0.127
ξ_{MR} (Yao)	0.0780	0.095	0.115

observations can be made: 1) IDT is reduced with increase in the ambient temperature for both mechanisms, and 2) with increase in the ambient temperature, the most reactive mixture fraction (ξ_{MR}) shifts towards the richer side for both mechanisms. Accordingly, the respective ξ_{MR} values for Polimi are larger than for Yao as reported in Table 2.

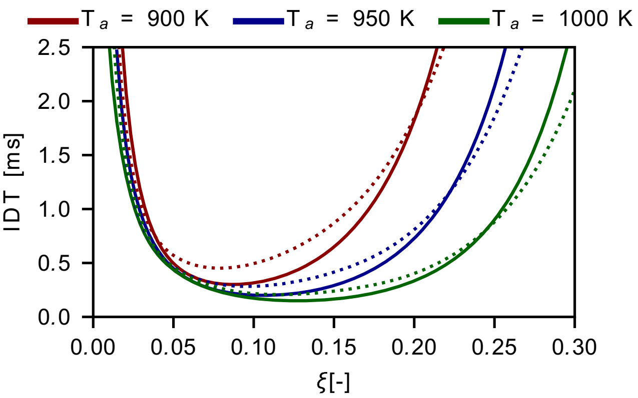

Figure 3. 0D homogeneous reactor calculations: IDT against ξ under spray A conditions for n-dodecane/methane using Polimi (solid) and Yao (dotted) at different ambient temperatures.

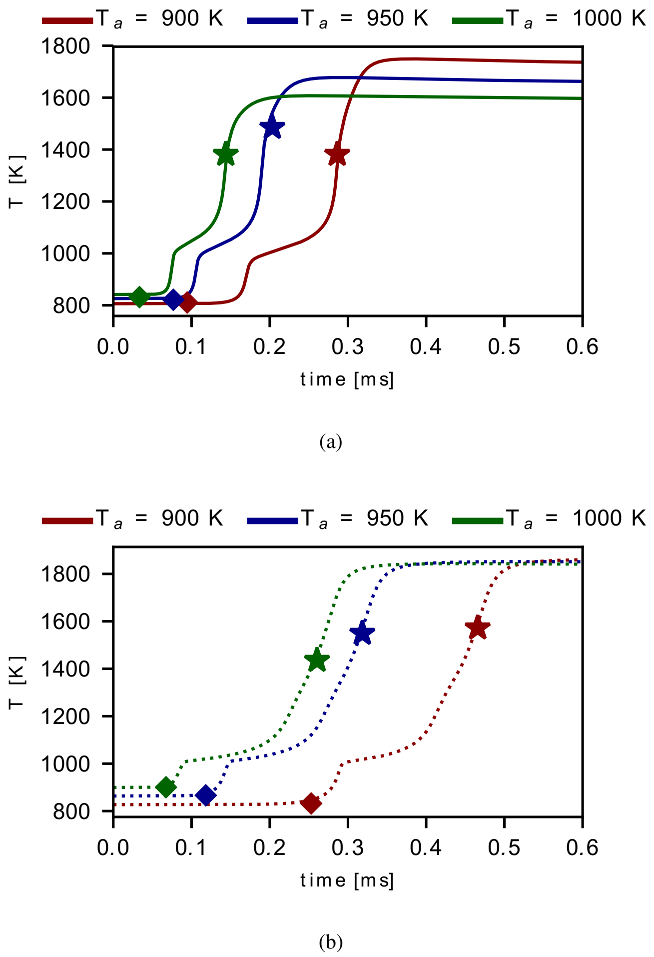

(a)

(b)

Figure 4. Temporal evolution of temperature using 0D homogeneous reactor calculations: (a) Polimi (b) Yao for n-dodecane/methane ignition at different ambient temperatures. Here, τ_1 and τ_2 are marked with diamond and star symbols, respectively.

Figure 4 displays progress of temperature with time in 0D homogeneous reactor simulations at ξ_{MR} wherein first-stage IDT and second-stage IDT are marked with symbols. It is observed that for Yao, the first-stage IDT is longer than in Polimi at different ambient temperatures as consistent with the observations in Refs.[2,3,35]. This delay in the first-stage IDT leads to later second-stage IDT in cases with Yao mechanism, c.f. Table 3. We note that in Figure 4, there is an evident difference in the final products temperature with T_a increase for Polimi, whereas for Yao this trend is not present. We note that the aforementioned difference in the most reactive mixture fractions between the two mechanisms leads to different initial temperature and consequently, different final temperature in Figures 4 (a) and (b). It should be mentioned that this effect does not happen in 3D LES results, presented in the following section, since the most reactive mixture fraction and the mixing line concepts are not used in 3D LES.

To shed light on the reasons for difference in IDT between Polimi and Yao cases, a reaction sensitivity analysis has been performed earlier at 900 K ambient temperature with the two mechanisms by Kahila et al.[35] using 0D numerical simulations. We refer to that study wherein both the SF (single-fuel n-dodecane) and DF ignition chemistry are shown to be dictated by reactions involving n-dodecane and its long hydrocarbon radical products. However in DF ignition, methane is shown to consume OH radicals required to initiate LTC reactions throughout reactions like $CH_4 + OH \rightarrow CH_3 + H_2O$ and chain terminating reactions like $CH_3 + HO_2 \rightarrow CH_4 + O_2$ and $2\,CH_3(+M) \rightarrow C_2H_6(+M)$. In both Polimi and Yao, these chain terminating reactions are present but for Polimi, their inhibiting influence is shadowed by reactions involved in the early n-dodecane decomposition. Such an effect is considered as the main reason for the shorter IDT of the DF ignition with Polimi compared to Yao. According to[3], Yao overpredicts DF ignition while Polimi provides more realistic ignition results. We note that the aforementioned difference in reactions contribution to DF ignition with Yao and Polimi leads to differences in the most reactive mixture fraction in 0D simulations as reported in Table 2.

3D spray ignition

In DF ignition, species such as RO_2, HO_2, H_2O_2, and OH are considered for quantification of the ignition process. In particular, RO_2 is an important intermediate radical in decomposition of n-dodecane, and it can be used to mark the first-stage IDT. In contrast, OH is associated with high-temperature combustion, therefore used here to represent the second-stage ignition. Temporal evolution of maximum RO_2 mass fraction ($RO_{2\mathrm{max}}$) and OH mass fraction (OH_{max})

in different DF LES cases are presented in Figure 5 for Polimi (a) Yao (b). It is observed that at higher T_a, more RO_2 and OH are generated during the first-stage and second-stage ignition, respectively. Also, the first-stage and second-stage IDT variations with T_a present similar trends to those observed in Figure 4. In summary, (I) the higher ambient temperature leads to the earlier first-stage and second-stage ignition, (II) the ignition process is shorter with Polimi compared to Yao, and (III) RO_2 formation during the first-stage ignition is stronger with Yao compared to Polimi.

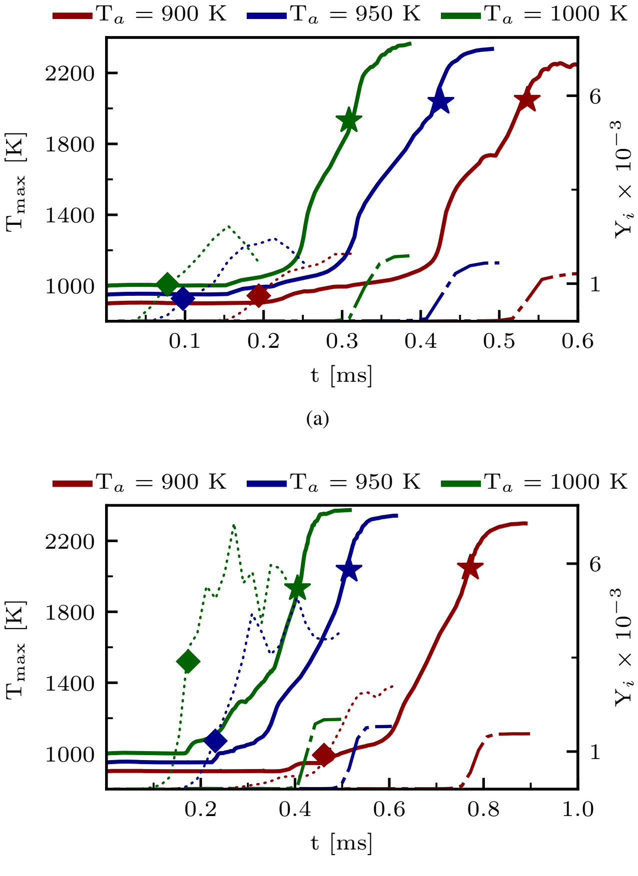

(a)

(b)

Figure 5. Temporal evolution of T_{max} (solid), RO_{2max}(dotted), and OH_{max}(dash-dotted line) in DF LES for a) Polimi b) Yao chemical mechanims. Here, τ_1 and τ_2 are marked with diamond and star symbols, respectively.

Table 3 summarizes the calculated first-stage and second-stage IDT for the carried out 0D and 3D LES cases in this study using Polimi and Yao mechanisms. Longer ignition delay time (IDT) is observed in 3D LES spray cases compared to 0D homogeneous reactors, due to the time needed for fuel mixing in 3D LES sprays. We note that in comparison between the 0D and 3D results, only the similarity of trends are of importance and a quantitative comparison is not possible; c.f.[2,3] for further details.

Figure 6 illustrates cut-planes of mixture fraction spatial distribution in 3D LES case studies at 1.1 τ_2. Moreover, iso-contours of stoichiometric mixture fraction and important intermediate species, RO_{2max} and H_2O_{2max} (relevant to LTC), and OH_{max} (relevant to HTC) are highlighted. It is noted that ignition typically starts from the spray tip region. Also, concentrations of LTC- and HTC-related species are stronger at higher T_a, which is consistent with the observations in Figure 5. According to Figure 6, at 900 K ambient temperature, spray volume is larger for Yao compared to Polimi, which is related to the longer IDT of the Yao mechanism compared to Polimi, as previously discussed. Accordingly, there is a higher level of mixing and dilution of the fuel spray for Yao case at T_a=900 K compared to Polimi. We note two reasons for different location of OH iso-lines in Yao and Polimi cases at T_a=900 K: 1) the sprays are shown at their respective $1.1\tau_2$ in Figure 6, i.e. a later physical time for Yao case compared to Polimi, 2) different reactions contributing to OH consumption in the Polimi and Yao cases, which was earlier discussed. We should note that this discrepancy between Polimi and Yao cases is weaker at higher ambient temperatures i.e 950 and 1000 K.

Table 3. Ignition delay time calculations from 0D homogeneous reactor calculations at ξ_{MR} and 3D LES (ms)

Cases	τ_1(0D)	τ_2(0D)	τ_1(LES)	τ_2(LES)
900 K (Polimi)	0.094	0.286	0.193	0.535
950 K (Polimi)	0.076	0.203	0.097	0.425
1000 K (Polimi)	0.033	0.143	0.077	0.308
900 K (Yao)	0.252	0.459	0.461	0.771
950 K (Yao)	0.118	0.318	0.230	0.514
1000 K (Yao)	0.067	0.270	0.173	0.405

Heat release mode analysis

In Figures 7 and 8, the total HRR is decomposed into different HRR modes based on the selection criteria defined for RO_2, H_2O_2, and OH mass fractions as well as temperature. The considered selection criteria are reported in Table 4 following the criteria set by Kahila et al.[2]. Here, the HRR modes are called early LTC, LTC, pre-HTC, HTC pre-ignition and HTC. Each HRR mode is integrated over the spray volume, which is defined as $\xi > 10^{-4}$. Here, time is normalized by the respective IDT in each LES case. Moreover, temporally integrated HRR modes are shown with pie-charts in Figures 7 and 8 to demonstrate the time-integrated contribution of each mode to the total HRR in percentage, within the period from the initial time till $1.1\tau_2$.

Table 4. Selected criteria for the HRR modes, the corresponding values used are $RO_{2crit} = 10^{-5}$, $H_2O_{2crit} = 10^{-4}$, $OH_{crit} = 10^{-5}$, $T_{crit} = 1150$ K.

Mode	Definitions
Early LTC	$(RO_2 \geq 1.10^{-7}) \cap (H_2O_2 \leq H_2O_{2crit}) \cap (T \leq T_{crit})$
LTC	$(RO_2 \geq (RO_{2crit})) \cap (H_2O_2 \geq H_2O_{2crit}) \cap (T \leq T_{crit})$
Pre-HTC	$(RO_2 < (RO_{2crit})) \cap (H_2O_2 \geq H_2O_{2crit}) \cap (T \leq T_{crit})$
HTC pre-ign	$(OH < OH_{crit}) \cap (T \leq T_{crit})$
HTC	$(OH \geq OH_{crit}) \cap (T \leq T_{crit})$

According to Figure 7, the LTC mode starts later in time and it is locally stronger for the Yao mechanism compared to the Polimi mechanism. However, the time-integrated LTC contribution to the total HRR is slightly stronger for the Polimi case than for the Yao case. This is consistent with the observations by Kahila et al.[2] at 900 K ambient temperature in which the Yao and Polimi cases have significant deviations in capturing the LTC mode. On the other hand, the time-integrated HTC mode contribution to the total HRR is considerably stronger for the Yao case,

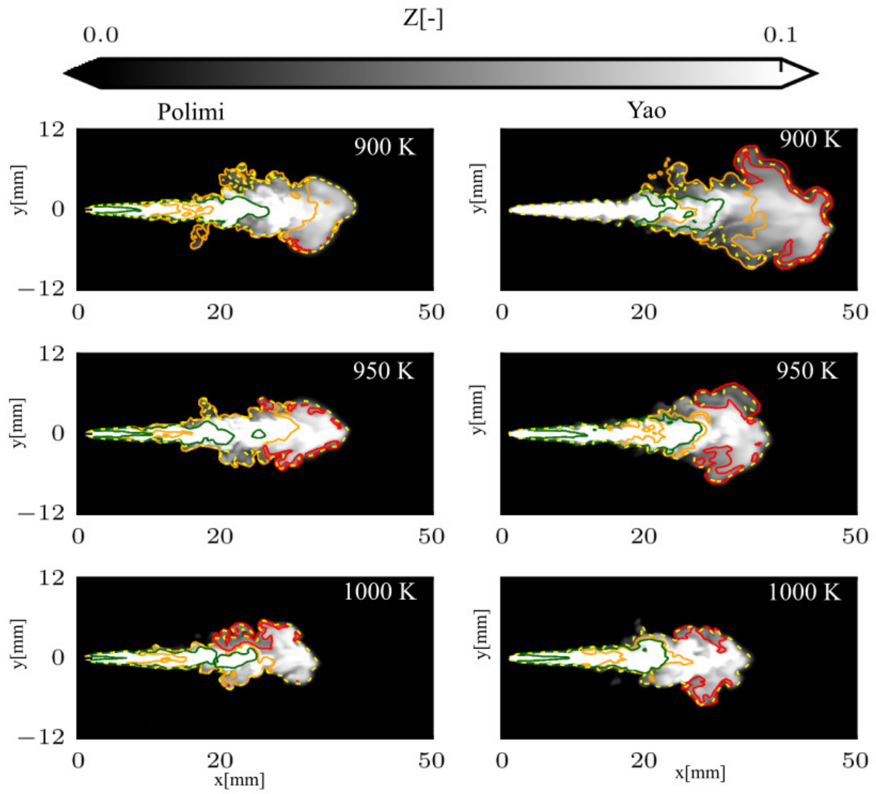

Figure 6. Spatial distribution of mixture fraction (ξ) at $1.1\tau_2$ using DF LES for Polimi (left) and Yao (right) chemical mechanisms. Iso-lines of stoichiometric ξ (dotted-yellow), 1 % RO_{2max} (solid-green), 25 % H_2O_{2max} (solid-orange) and 15 % OH_{max} (solid-red) are highlighted in the figure.

whereas the contribution of the time-integrated HTC pre-ignition mode is stronger for the Polimi case compared to the Yao case.

In Figure 8, i.e. 950 K ambient temperature, both local and time-integrated HRR modes have smaller differences for the two mechanisms compared to the cases at 900 K ambient temperature in Figure 7. Smaller differences in the HRR modes at higher ambient temperatures are correlated to the similarity of spray volumes at higher ambient temperatures as observed earlier in Figure 6 as well as smaller differences in IDT at higher ambient temperatures, c.f. Table 3. However, similar to the observation in Figure 7 at 900 K ambient temperature, the LTC mode is delayed in time and it is locally stronger for the Yao mechanism at 950 K ambient temperature.

We note that there is no experimental data on DF ignition under engine-relevant conditions and as there is no chemical kinetics mechanism developed for such DF conditions, it is not straightforward to recommend a chemical mechanism based on the current results. We note that although the Yao mechanism is preferred in expensive computations of 3D LES due to its lighter mechanism, the Polimi mechanism predicts ignition timing with a better accuracy. However, deviations in ignition characteristics and HRR modes between the Yao and Polimi mechanisms are smaller at higher ambient temperatures (950 K and 1000 K here). This trend justifies the use of Yao mechanism in future numerical simulations for DF ignition, especially at higher ambient temperatures.

Conclusions

In a modified dual-fuel (DF) ECN Spray A setup, ignition characteristics of n-dodecane spray into a lean methane-air mixture were investigated using 3D large eddy simulations (LES) and 0D homogeneous reactor calculations using the adiabatic mixing line. Two different chemical mechanisms, namely Yao (a skeletal mechanism with 54 species and 269 reaction steps) and Polimi (a reduced mechanism with 96 species and 993 reaction steps) were utilized. Three values of premixed gas ambient temperatures (T_a) were considered: 900, 950, and 1000 K. Ignition characteristics were investigated through analysis of the first- and second-stage ignition delay time (IDT) as well as low- and high-temperature chemistry (LTC and HTC). Several differences for Yao and Polimi in prediction of IDT, LTC, and HTC were observed. The main findings of this study are highlighted in the following.

1. According to both 0D homogeneous reactor calculations and 3D LES simulations, the choice of chemical mechanism can influence ignition characteristics and modes of combustion specifically at lower T_a. At T_a=900 K, deviations between the case studies with two different mechanisms are more pronounced compared to the cases at T_a=1000 K.
2. Yao mechanism overpredicts first- and second-stage IDT values compared to Polimi mechanism. This trend is stronger at lower T_a, i.e. 900 K. In both Polimi and Yao, chain terminating reactions are present which consume OH, but for Polimi their inhibiting influence

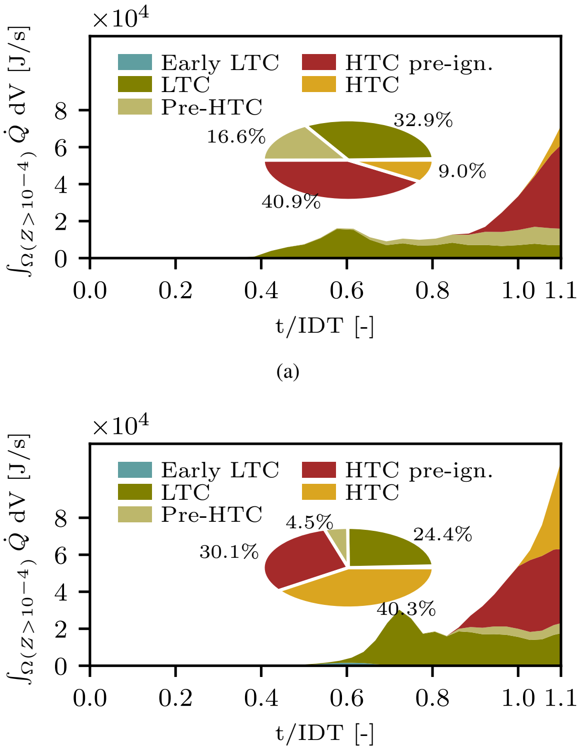

(a)

(b)

Figure 7. Modal decomposition of the total HRR within the spray region for n-dodecane/methane for (a) Polimi mechanism (b) Yao mechanism at ambient temperature 900 K. Here, time is normalized with the respective IDT in each case. The pie-charts represent the time-integrated contribution of each mode from the start of injection until 1.1τ_2.

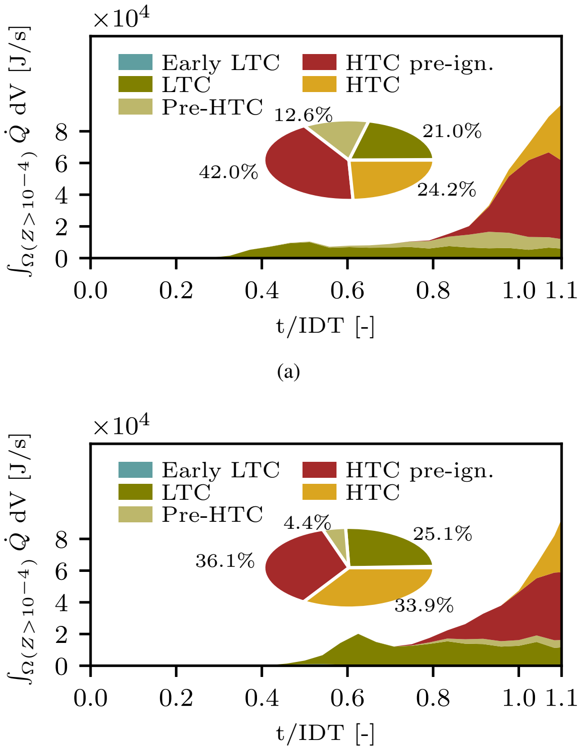

(a)

(b)

Figure 8. Modal decomposition of the total HRR within the spray region for n-dodecane/methane for (a)Polimi mechanism (b) Yao mechanism at ambient temperature 950 K. Here, time is normalized with the respective IDT in each case. The pie-charts represent the time-integrated contribution of each mode from the start of injection until 1.1τ_2.

is shadowed by reactions involved in the early n-dodecane decomposition.

3. Due to the longer IDT values for Yao mechanism at lower T_a compared to Polimi, the spray volume is observed to be larger at the time of ignition. Therefore, there is longer time for mixing before the first instance of ignition for Yao at T_a=900 K compared to Polimi. Such an effect leads to different distribution of intermediate radicals for Yao and Polimi cases at 900 K ambient temperature.
4. Modes of heat release rate (HRR) analysis indicates that the LTC region is delayed and it is locally stronger for Yao compared to Polimi mechanism at 900 K ambient temperature. In particular at 900 K ambient temperature, Polimi and Yao show significant differences in capturing the LTC mode which leads to different first-stage and consequently, second-stage IDT. Similar to the trends observed for IDT, at higher T_a (950 K), the time-integrated contributions of combustion modes are similar for the two mechanisms.

Acknowledgments

This study is financially supported by the Academy of Finland (grant numbers 318024 and 297248). We acknowledge CSC (Finnish IT Center for Science) for providing the computational resources. Furthermore, the first author has been financially supported by the Merenkulun Säätiö.

Declaration of conflicting interests

The author(s) declared no potential conflicts of interest with respect to the research, authorship, and/or publication of this article.

APPENDIX A: Mesh sensitivity study

In this appendix, a mesh sensitivity analysis is carried out to elaborate on the sensitivity of the provided results in this study to the selected mesh. Here, the DF n-dodecane/methane case at T_a=1000 K with Polimi is selected for the mesh sensitivity analysis. With reference to Figure 1, here the R3 region is replaced with a finer grid spacing. In particular, the standard 125-micron grid spacing used in this study in the R3 region is replaced by a 62.5-micron grid spacing mesh.

Results of the mesh sensitivity analysis are presented in Figure 9, wherein temporal evolution of T_{max} (solid), maximum RO_2 mass fraction (RO_{2max})(dotted) and OH mass fraction (OH_{max})(dotted line) are displayed. It is observed that there are small deviations between the results of the standard mesh (minimum grid spacing of 125 micron) compared to the finer mesh (minimum grid spacing of 62.5

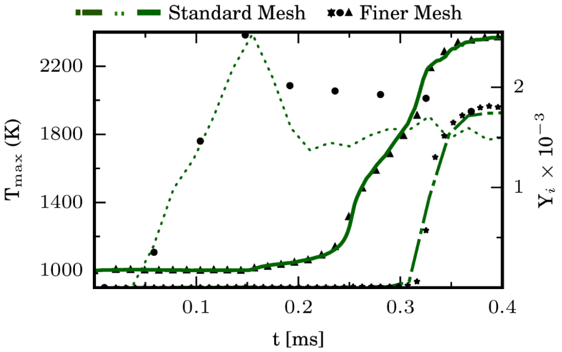

Figure 9. Mesh sensitivity analysis for 125 micron mesh (lines) and 62.5 micron mesh (symbols) in DF LES using Polimi at the ambient temperature of 1000 K. Here, the different lines represent $T_{\max}$ (solid), $RO_{2\max}$(dotted) and $OH_{\max}$(dash-dotted line) respectively.

Table 5. IDT values for standard and finer mesh cases at 1000 K ambient temperature using Polimi mechanism

Cases	τ_1(LES)	τ_2(LES)
1000 K (Standard mesh)	0.033	0.308
1000 K (Finer mesh)	0.067	0.325

micron). Table 5 presents the IDT values for the standard and finer mesh configurations, wherein it is observed that the second-stage IDT values are not sensitive to the mesh resolution. However, we note that the first-stage IDT is more sensitive to the mesh resolution, which is mainly relevant to high fluctuations of the intermediate species in LTC-related reactions. Therefore, the utilized standard mesh resolution in this study is considered to be promising for achieving grid-independent results.

APPENDIX B: Information on computational resources.

The present work is carried out using the PUHTI Atos BullSequana X400 supercomputer in Finland. PUHTI has a total of 682 CPU nodes and latest generation Intel Xeon Gold 6230 processors running at 2.1 GHz speed. The computational load for present simulations has been reported in Figure 10. The computational cost for using the Polimi mechanism is higher than that for the Yao mechanism, due to its higher number of species and reaction steps. In addition, it can be observed that the computational cost in early iterations is lower for all cases. This is due to existence of both less-stiff/chemically inert conditions within earlier iterations.

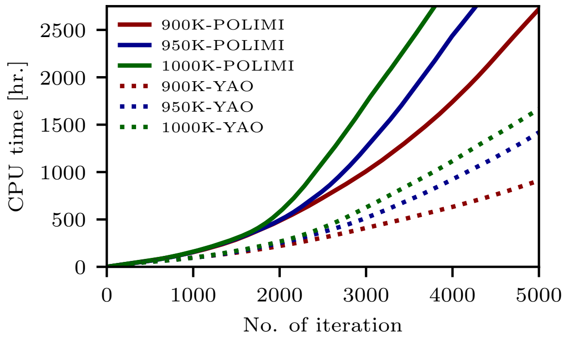

Figure 10. The computational load for present LES simulations comparing Polimi and Yao mechanisms.

References

1. Reitz RD. Directions in internal combustion engine research. *Combustion and Flame* 2013; 160(1): 1–8.
2. Kahila H, Kaario O, Ahmad Z et al. A large-eddy simulation study on the influence of diesel pilot spray quantity on methane-air flame initiation. *Combustion and Flame* 2019; 206: 506–521. DOI: 10.1016/J.COMBUSTFLAME.2019.05.025. URL `https://www.sciencedirect.com/science/article/pii/S001021801930238X?via{%}3Dihub`.
3. Tekgül B, Kahila H, Kaario O et al. Large-eddy simulation of dual-fuel spray ignition at different ambient temperatures. *Combustion and Flame* 2020; DOI:10.1016/j.combustflame.2020.01.017.
4. Momenimovahed A, Liu F, Thomson KA et al. Effect of fuel composition on properties of particles emitted from a diesel–natural gas dual fuel engine. *International Journal of Engine Research* 0; 0(0): 1468087419846018. DOI:10.1177/1468087419846018. URL `https://doi.org/10.1177/1468087419846018`. `https://doi.org/10.1177/1468087419846018`.
5. Lee J, Chu S, Kang J et al. The classification of gasoline/diesel dual-fuel combustion based on the heat release rate shapes and its application in a light-duty single-cylinder engine. *International Journal of Engine Research* 2019; 20(1): 69–79. DOI:10.1177/1468087418817676. URL `https://doi.org/10.1177/1468087418817676`. `https://doi.org/10.1177/1468087418817676`.
6. Bhattacharya A and Basu S. An investigation into the heat release and emissions from counterflow diffusion flames of methane/dimethyl ether/hydrogen blends in air. *International Journal of Hydrogen Energy* 2019; 44(39): 22328 – 22346. DOI:https://doi.org/10.1016/j.ijhydene.2019.06.190. URL `http://www.sciencedirect.com/science/article/pii/S0360319919324905`.
7. Wu Z, Rutland CJ and Han Z. Numerical evaluation of the effect of methane number on natural gas and diesel dual-fuel combustion. *International Journal of Engine Research* 2019; 20(4): 405–423. DOI:10.1177/1468087418758114.
8. Dai XH, Singh S, Krishnan SR et al. Numerical study of combustion characteristics and emissions of a diesel–methane dual-fuel engine for a wide range of injection timings. *International Journal of Engine Research* 2020; 21(5): 781–793. DOI:10.1177/1468087418783637.
9. Bermúdez V, Macián V, Villalta D et al. Impact of injection settings on gaseous emissions and particle size distribution in the dual-mode dual-fuel concept. *International Journal of Engine Research* 2020; 21(4): 561–577. DOI:10.1177/1468087419844413.
10. Rochussen J and Kirchen P. Characterization of reaction zone growth in an optically accessible heavy-duty diesel/methane dual-fuel engine. *International Journal of Engine Research* 2019; 20(5): 483–500. DOI:10.1177/1468087418756538. URL `https://doi.org/10.`

1177/1468087418756538. https://doi.org/10.1177/1468087418756538.

11. Korkmaz M, Ritter D, Jochim B et al. Effects of injection strategy on performance and emissions metrics in a diesel/methane dual-fuel single-cylinder compression ignition engine. *International Journal of Engine Research* 2019; 20(10): 1059–1072. DOI:10.1177/1468087419836586. URL https://doi.org/10.1177/1468087419836586. https://doi.org/10.1177/1468087419836586.
12. Pei Y, Davis MJ, Pickett LM et al. Engine Combustion Network (ECN): Global sensitivity analysis of Spray A for different combustion vessels. *Combustion and Flame* 2015; 162(6): 2337–2347. DOI:10.1016/j.combustflame.2015.01.024. URL http://dx.doi.org/10.1016/j.combustflame.2015.01.024.
13. Pei Y, Som S, Kundu P et al. Large Eddy Simulation of a Reacting Spray Flame under Diesel Engine Conditions. *SAE Technical Papers* 2015; 2015-Septe. DOI:10.4271/2015-01-1844.
14. Pei Y, Som S, Pomraning E et al. Large eddy simulation of a reacting spray flame with multiple realizations under compression ignition engine conditions. *Combustion and Flame* 2015; 162(12): 4442–4455. DOI:10.1016/J.COMBUSTFLAME.2015.08.010. URL https://www.sciencedirect.com/science/article/pii/S0010218015002710?via{%}3Dihub.
15. Bolla M, Chishty MA, Hawkes ER et al. Modeling combustion under engine combustion network Spray A conditions with multiple injections using the transported probability density function method. *International Journal of Engine Research* 2017; 18(1-2): 6–14. DOI:10.1177/1468087416689174.
16. Xu C, Ameen MM, Som S et al. Dynamic adaptive combustion modeling of spray flames based on chemical explosive mode analysis. *Combustion and Flame* 2018; 195: 30–39. DOI:10.1016/j.combustflame.2018.05.019. URL https://doi.org/10.1016/j.combustflame.2018.05.019.
17. Kahila H, Wehrfritz A, Kaario O et al. Large-eddy simulation on the influence of injection pressure in reacting Spray A. *Combustion and Flame* 2018; 191: 142–159. DOI:10.1016/J.COMBUSTFLAME.2018.01.004. URL https://www.sciencedirect.com/science/article/pii/S0010218018300087?via{%}3Dihub.
18. Cho HM and He BQ. Spark ignition natural gas engines—A review. *Energy Conversion and Management* 2007; 48(2): 608–618. DOI:10.1016/J.ENCONMAN.2006.05.023. URL https://www.sciencedirect.com/science/article/pii/S0196890406001919?via{%}3Dihub.
19. Korakianitis T, Namasivayam A and Crookes R. Natural-gas fueled spark-ignition (SI) and compression-ignition (CI) engine performance and emissions. *Progress in Energy and Combustion Science* 2011; 37(1): 89–112. DOI:10.1016/J.PECS.2010.04.002. URL https://www.sciencedirect.com/science/article/pii/S0360128510000377?via{%}3Dihub.
20. Pickett LM, Genzale CL, Bruneaux G et al. Comparison of diesel spray combustion in different high-temperature, high-pressure facilities. *SAE Technical Papers* 2010; 3(2): 156–181. DOI:10.4271/2010-01-2106.
21. Maes N, Meijer M, Dam N et al. Characterization of Spray A flame structure for parametric variations in ECN constant-volume vessels using chemiluminescence and laser-induced fluorescence. *Combustion and Flame* 2016; 174: 138–151. DOI:10.1016/j.combustflame.2016.09.005. URL http://dx.doi.org/10.1016/j.combustflame.2016.09.005.
22. Skeen SA, Manin J and Pickett LM. Simultaneous formaldehyde PLIF and high-speed schlieren imaging for ignition visualization in high-pressure spray flames. *Proceedings of the Combustion Institute* 2015; 35(3): 3167–3174. DOI:10.1016/j.proci.2014.06.040. URL http://dx.doi.org/10.1016/j.proci.2014.06.040.
23. Skeen S, Manin J and Pickett LM. Visualization of Ignition Processes in High-Pressure Sprays with Multiple Injections of n-Dodecane. *SAE International Journal of Engines* 2015; 8(2): 696–715. DOI:10.4271/2015-01-0799.
24. Schlatter S, Schneider B, Wright YM et al. N-heptane micro pilot assisted methane combustion in a Rapid Compression Expansion Machine. *Fuel* 2016; 179: 339–352. DOI:10.1016/J.FUEL.2016.03.006. URL https://www.sciencedirect.com/science/article/pii/S0016236116300369.
25. Srna A, Bruneaux G, Von Rotz B et al. Optical investigation of sooting propensity of n-dodecane pilot/lean-premixed methane dual-fuel combustion in a rapid compression-expansion machine. *SAE International Journal of Engines* 2018; 11(6): 1049–1068.
26. Kokjohn SL, Hanson RM, Splitter DA et al. Fuel reactivity controlled compression ignition (RCCI): A pathway to controlled high-efficiency clean combustion. *International Journal of Engine Research* 2011; 12(3): 209–226. DOI:10.1177/1468087411401548.
27. Nieman DE, Dempsey AB and Reitz RD. Heavy-Duty RCCI Operation Using Natural Gas and Diesel. *SAE International Journal of Engines* 2012; 5(2): 270–285. DOI:10.4271/2012-01-0379.
28. Karim GA. Combustion in gas fueled compression: Ignition engines of the dual fuel type. *Journal of Engineering for Gas Turbines and Power* 2003; 125(3): 827–836. DOI:10.1115/1.1581894.
29. Li J, Yang WM, Goh TN et al. Study on RCCI (reactivity controlled compression ignition) engine by means of statistical experimental design. *Energy* 2014; 78: 777–787. DOI:10.1016/J.ENERGY.2014.10.071. URL https://www.sciencedirect.com/science/article/pii/S0360544214012213?via{%}3Dihub.
30. Bhagatwala A, Sankaran R, Kokjohn S et al. Numerical investigation of spontaneous flame propagation under RCCI conditions. *Combustion and Flame* 2015; 162(9): 3412–3426. DOI:10.1016/J.COMBUSTFLAME.2015.06.005. URL https://www.sciencedirect.com/science/article/pii/S0010218015001844?via{%}3Dihub.
31. Masouleh] MG, Wehrfritz A, Kaario O et al. Comparative study on chemical kinetic schemes for dual-fuel combustion of n-dodecane/methane blends. *Fuel* 2017; 191: 62 – 76. DOI:https://doi.org/10.1016/j.fuel.2016.10.114. URL http://www.sciencedirect.com/science/article/pii/S001623611631078X.
32. Demosthenous E, Borghesi G, Mastorakos E et al. Direct Numerical Simulations of premixed methane flame initiation by pilot n-heptane spray autoignition.

Combustion and Flame 2016; 163: 122–137. DOI: 10.1016/J.COMBUSTFLAME.2015.09.013. URL https://www.sciencedirect.com/science/article/pii/S0010218015003168?via{%}3Dihub.

33. Wang Z and Abraham J. Fundamental physics of flame development in an autoigniting dual fuel mixture. *Proceedings of the Combustion Institute* 2015; 35(1): 1041–1048. DOI:10.1016/J.PROCI.2014.06.079. URL https://www.sciencedirect.com/science/article/pii/S1540748914002375?via{%}3Dihub.
34. Li Y, Jia M, Chang Y et al. Parametric study and optimization of a RCCI (reactivity controlled compression ignition) engine fueled with methanol and diesel. *Energy* 2014; 65: 319–332. DOI:10.1016/J.ENERGY.2013.11.059. URL https://www.sciencedirect.com/science/article/pii/S0360544213010293.
35. Kahila H, Wehrfritz A, Kaario O et al. Large-eddy simulation of dual-fuel ignition: Diesel spray injection into a lean methane-air mixture. *Combustion and Flame* 2019; 199: 131–151. DOI:10.1016/j.combustflame.2018.10.014.
36. Wehrfritz A, Vuorinen V, Kaario O et al. Large eddy simulation of high-velocity fuel sprays: studying mesh resolution and breakup model effects for spray a. *Atomization and Sprays* 2013; 23(5).
37. Wehrfritz A, Kaario O, Vuorinen V et al. Large Eddy Simulation of n-dodecane spray flames using Flamelet Generated Manifolds. *Combustion and Flame* 2016; 167: 113–131. DOI:10.1016/J.COMBUSTFLAME.2016.02.019. URL https://www.sciencedirect.com/science/article/pii/S0010218016000754?via{%}3Dihub.
38. Gadalla M, Kannan J, Tekgül B et al. Large-eddy simulation of ecn spray a: Sensitivity study on modeling assumptions. *Energies* 2020; 13(13). DOI:10.3390/en13133360. URL https://www.mdpi.com/1996-1073/13/13/3360.
39. Weller HG, Tabor G, Jasak H et al. A tensorial approach to computational continuum mechanics using object-oriented techniques. *Computers in physics* 1998; 12(6): 620–631.
40. Senecal P, Pomraning E, Xue Q et al. Large eddy simulation of vaporizing sprays considering multi-injection averaging and grid-convergent mesh resolution. *Journal of Engineering for Gas Turbines and Power* 2014; 136(11).
41. Jasak H, Weller H and Gosman A. High resolution nvd differencing scheme for arbitrarily unstructured meshes. *International journal for numerical methods in fluids* 1999; 31(2): 431–449.
42. Kaario OT, Vuorinen V, Kahila H et al. The effect of fuel on high velocity evaporating fuel sprays: Large-Eddy simulation of Spray A with various fuels. *International Journal of Engine Research* 2020; 21(1): 26–42. DOI:10.1177/1468087419854235.
43. Ranz W, Marshall WR et al. Evaporation from drops. *Chem eng prog* 1952; 48(3): 141–146.
44. Froessling N. Evaporation, heat transfer, and velocity distribution in two-dimensional and rotationally symmetrical laminar boundary-layer flow 1958; .
45. Niemeyer KE, Curtis NJ and Sung CJ. pyjac: Analytical jacobian generator for chemical kinetics. *Computer Physics Communications* 2017; 215: 188–203.
46. Yao T, Pei Y, Zhong BJ et al. A compact skeletal mechanism for n-dodecane with optimized semi-global low-temperature chemistry for diesel engine simulations. *Fuel* 2017; 191: 339–349. DOI:10.1016/J.FUEL.2016.11.083. URL https://www.sciencedirect.com/science/article/pii/S001623611631184X?via{%}3Dihub.
47. Frassoldati A, D'Errico G, Lucchini T et al. Reduced kinetic mechanisms of diesel fuel surrogate for engine CFD simulations. *Combustion and Flame* 2015; 162(10): 3991–4007. DOI:10.1016/J.COMBUSTFLAME.2015.07.039. URL https://www.sciencedirect.com/science/article/pii/S0010218015002473?via{%}3Dihub.
48. Karimkashi S, Kahila H, Kaario O et al. A numerical study on combustion mode characterization for locally stratified dual-fuel mixtures. *Combustion and Flame* 2020; 214: 121–135. DOI:10.1016/J.COMBUSTFLAME.2019.12.030. URL https://www.sciencedirect.com/science/article/pii/S0010218019305826?via{%}3Dihub.
49. Karimkashi S, Kahila H, Kaario O et al. Numerical study on tri-fuel combustion: Ignition properties of hydrogen-enriched methane-diesel and methanol-diesel mixtures. *International Journal of Hydrogen Energy* 2020; DOI:10.1016/J.IJHYDENE.2019.12.033. URL https://www.sciencedirect.com/science/article/pii/S0360319919345331?via{%}3Dihub.
50. Westbrook CK. Chemical kinetics of hydrocarbon ignition in practical combustion systems. *Proceedings of the Combustion Institute* 2000; 28(2): 1563 – 1577. DOI: https://doi.org/10.1016/S0082-0784(00)80554-8. URL http://www.sciencedirect.com/science/article/pii/S0082078400805548.
51. Mastorakos E. Ignition of turbulent non-premixed flames. *Progress in Energy and Combustion Science* 2009; 35(1): 57–97. DOI:10.1016/J.PECS.2008.07.002. URL https://www.sciencedirect.com/science/article/pii/S0360128508000415?via{%}3Dihub.
52. Bilger R, Stårner S and Kee R. On reduced mechanisms for methaneair combustion in nonpremixed flames. *Combustion and Flame* 1990; 80(2): 135 – 149. DOI: https://doi.org/10.1016/0010-2180(90)90122-8. URL http://www.sciencedirect.com/science/article/pii/001021809090122S.